RSC Advances

1

2

1 **Hydrothermal effect on synthesis, characterization and catalytic**
2 **properties of calcium methoxide for biodiesel production from**
3 **crude *Jatropha curcus***
4

5 Siow Hwa Teo,[ab] Yun Hin Taufiq-Yap[ab], Umer Rashid[c] and Aminul Islam[ab]

6

7 [a]*Catalysis Science and Technology Research Centre, Faculty of Science, Universiti Putra*

8 *Malaysia, 43400, Serdang, Selangor, Malaysia.*

9 [b]*Department of Chemistry, Faculty of Science, Universiti Putra Malaysia, 43400, Serdang,*

10 *Selangor, Malaysia.*

11 [c]*Institute of Advanced Technology, Universiti Putra Malaysia, 43400 UPM Serdang,*

12 *Selangor, Malaysia.*

13

14

15

16

17 Yun Hin Taufiq-Yap (**Corresponding author**)

18 Catalysis Science and Technology Research Centre,

19 Faculty of Science, Universiti Putra Malaysia, 43400

20 UPM Serdang, Selangor, Malaysia.

21 Tel: +603-89466809, Fax: +603-89466758,

22 Email: taufiq@upm.edu.my

23

24

25

26

27

28   Hydrothermal synthesis is well-suited approach for preparation of bulk metal catalysts which

29   showed high purity, cost-effective and easy for controlling (temperature and time). In the

30   current study, an effective catalyst for transesterification of high fatty acid content of crude

31   *Jatropha curcus* oil (JCO) was appraised. Calcium methoxide ($Ca(OCH_3)_2$) has been

32   successfully synthesized via a green and economic hydrothermal process at different time.

33   CaO was used precursor as it is abundance, inexpensive and environmental friendly.

34    $Ca(OCH_3)_2$ can form on the surface of CaO and its active basic surface is very well

35   developed. This facile experimental strategy without any surfactant or template produced

36   porous $Ca(OCH_3)_2$ along with a high surface area and highly basicity, which leads to a

37   superior catalytic reaction and proves to be a promising alternative for short reaction time

38   solid based catalyst in biodiesel production in term of excellent transesterification

39   performance and long durability. The performance of synthesized $Ca(OCH_3)_2$ was examined

40   by characterizing it using analytical techniques such as TG-DTA, XRD, BET, FT-IR, TEM

41   and SEM. $Ca(OCH_3)_2$ catalysts gave raised 3 types of morphologies *i.e* (a) irregular round

42   shape particles, (b) a well arrangement of plate-like structures with rough surface and (c) a

43   cluster of tiny plate-like architectures with smooth surface. The correlation between synthesis

44   time, surface area and morphology of catalysts on biodiesel yield were studied. $Ca(OCH_3)_2$

45   catalyst was able to maintain the FAME content above 86 % after fifth cycle, at optimum

46   reaction conditions: 2 h reaction time, 12: 1 methanol/ oil molar ratio, 2 wt.% catalyst loading

47   and 65 °C reaction temperature. $Ca(OCH_3)_2$ is a prevailing heterogeneous catalyst for

48   transesterification reaction of non-edible *Jatropha curcas* oil for biodiesel production.

49    $Ca(OCH_3)_2$ catalyst can be separated easily from the reaction mixture and reused to give a

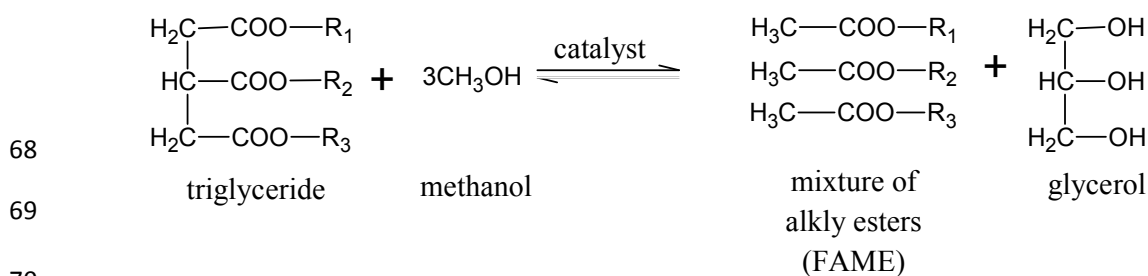50   consistent transesterification activity.

51   **Keywords**   Biodiesel   production;   *Jatropha   curcas*;   Heterogeneous   catalyst;

52   Transesterification; Calcium methoxide

Introduction

Biodiesel, also called fatty acid methyl ester (FAME) is a promising alternative energy source for transportation sector. Numerous advantages associated with biodiesel such as renewable, low/ zero net CO_2 emission, low sulfur and higher biodegradability.[1] Additionally, biodiesel is superior to fossil diesel fuel in terms of cetane number, flash point and lubricity characteristics. Biodiesel can be produced by transesterification with alcohol of various feedstocks such as vegetable oils (Europe), palm oil (South East Asia), *Jatropha* oil, Kranjar oil (India) and soybean oil (USA). In order to solve the problems related to the food-based biodiesel, non-edible oils have found increasing attention as potential feedstocks.[2]

Jatropha curcus. L consisting about 60 % oil content from seed kernel. It is found that the increasing attention of *Jatropha curcus* L as potential feedstock due to its non-edible, easy to produce, low cost and availability of seeds in abundance. Therefore, this makes its use as energy or fuel source very attractive especially for biodiesel production. The overall reaction of methanolysis of vegetable oils reaction is shown in Scheme 1.

R$_1$, R$_2$, R$_3$ = Hydrocarbon chain ranging from 15 to 21 carbon atoms

Scheme 1. Transesterification of triglyceride with methanol.

Due to the non-corrosion, environmental benignancy and easy separation from liquid products advantages, heterogeneous solid catalysts are being widely used for the

76   transesterification of triglycerides. Calcium oxide (CaO) is the most widely used and exhibit

77   good catalytic properties for transesterification of triglyceride to biodiesel, due to economic

78   point of view.[3,4] However, the reaction rate was slow and it seems to be not adaptable for

79   industry application as extensive leaching such as Ca^{2+} may intimidate the reusability and the

80   environment sustainability of catalyst.[5,6]

81   Recently, hydrothermal synthesis has turn out to be well-suited for preparation bulk

82   metal catalysts, which exhibited high purity, low cost and easy to control (*i.e.* temperature

83   and time). The main advantage to synthesize is due to variety of micro/nano-materials with

84   unique morphologies, such as nanocable,[7] nanoroad,[8] star-shaped and flower-like[9] products.

85   Up to now, this techniques has been successfully applied in preparing $Ca(OCH_3)_2$ solid

86   catalyst.[10,11,12]   However,   morphology   and   structure   controlled   growth   of   micro/

87   nanoarchitectures of $Ca(OCH_3)_2$, which exhibited various unique of physical and chemical

88   properties such as high surface area, ideal porosity and strong basicity. The nanoparticle

89   catalyst is an important factor to improve the catalytic properties by exposing catalytic active

90   $^-OCH_3$ predominantly on the surface of catalyst which favor for transesterification reaction.[13]

91   Herein, we report a simple hydrothermal approach without using any surfactant and

92   template to prepare $Ca(OCH_3)_2$ catalyst. By varying the synthesis time, heterogeneous

93   catalysts exhibiting different effectiveness in the transesterification of crude *Jatropha curcus*

94   oil (JCO) with methanol, have been obtained. The active phase of $Ca(OCH_3)_2$ was

95   characterized with data obtained from physico-chemical properties of the catalysts. The

96   influence of various synthesis time on the size, structural and textural of prepared $Ca(OCH_3)_2$

97   is appraised. Also, the correlative effect between transesterification activity and catalyst

98   surface area is discussed. Besides, this the first report on catalytic performance of $Ca(OCH_3)_2$

99   for the transesterification of non-edible crude JCO is presented. Moreover, the efficiency and

100 reusability of the catalyst in biodiesel production is also studied.

101 **EXPERIMENTAL**

102 **Preparation and characterization of materials**

103 Crude *Jatropha curcas* L. oil (JCO) was purchased from Bionas Sdn Bhd, Malaysia and was

104 used without further treatment and purification. CaO (R&M Chemicals, 99.0 %), anhydrous

105 methanol (Merch, 99.7 %) were purchased from Fisher Scientific and used for methanolysis

106 of CaO and transesterification of oil reactions. Dichloromethane (Fisher Scientific, UK) was

107 used as medium FAME yield test. Methyl heptadecanoate, $C_{18}H_{36}O_2$ internal standard for gas

108 chromatography analysis. All the chemicals used in the present study were analytical reagent

109 grade.

110 The fatty acid profile of crude JCO was identified and is tabulated in Table 1. The

111 average molecular weight (M) was calculated based on the acid value (AV) and

112 saponification value (SV) of crude JCO obtained using the following correlation as

113 following:[14]

114 M = 56.1 x 1000 x 3/ (SV - AV)   (1)

115 $Ca(OCH_3)_2$ catalyst was prepared by heating CaO in an excess dehydrated methanol

116 under 65 $^{\circ}$C at a range of durations (2 to 12 h) under N_2 flow (50 ml min^{-1}). The reaction can

117 be expressed by following (Scheme 2):

calcium oxide   calcium methoxide
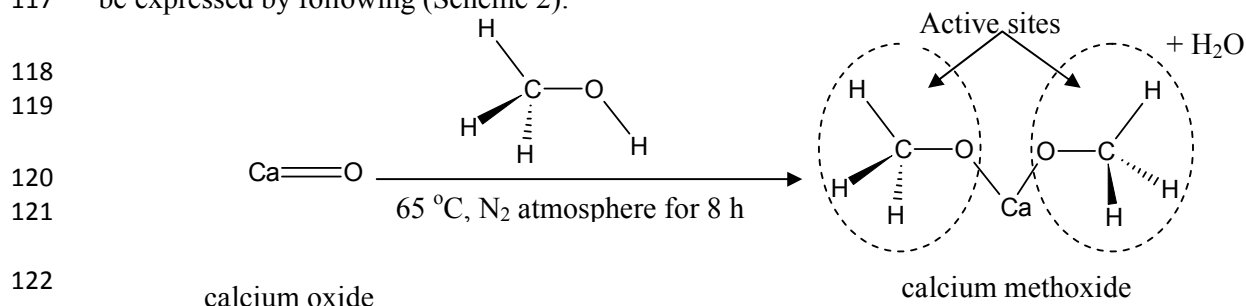
123 **Scheme 2** Hydrothermal of calcium oxide with methanol.

124 CaO was used without remove any hydroxide phase. Typically 1 g of CaO was

125 dispersed rapidly to the 20 ml of anhydrous methanol in a three-neck round bottom flask

126 equipped with a water-cooled reflux condenser and a magnetic stirrer. The resulting white

127   suspended slurry was undergoing a continuous stirring of 600 rpm to facilitate sufficient

128   contact between the reactants. Then, the white paste precursor was formed by distilled most

129   of methanol using a rotary evaporator under reduced pressure and dried in the vacuum oven

130   at 105 ^{o}C for 1 h. Henceforth, the catalysts were denoted as CM*X* , where *X* represents the

131   reflux time of 2, 4, 6, 8, 10 and 12 h, respectively.

132
133   **Catalysts characterization**

134   Thermogravimetric and differential thermal analysis (TG/DTA) of $Ca(OCH_3)_2$ catalysts were

135   performed using a Mettler Toledo thermogravimetric analyzer. The heating was carried out in

136   an air flow (100 ml min^{-1}) with heating rate 10 ^{o}C min^{-1}, from 35 to 1000 ^{o}C.

137   The powder X-ray diffraction analysis (XRD) was employed to identify the

138   crystallography of $Ca(OCH_3)_2$ catalysts. The analysis was carried out using a Shimadzu

139   diffracto-meter model XRD6000. The diffracto-meter employing CuKa radiation (2.7 kW

140   and 30 mA) with wavelength (λ) of 1.54 Å to generate diffraction patterns from powder

141   crystalline samples at ambient temperature. The data were recorded over a 2*θ* range of 5-40°

142   with a steps of 0.02^o and count time 1s. Each sample was run for 35 mins. The phases were

143   identified using the power diffraction file (PDF) database (JCPDS, International Centre for

144   Diffraction Data). The crystallite size of the catalysts can be calculated from the line

145   broadening or FWHM (full width at half maximum) of corresponding peaks (the most intense

146   peaks), which is by using Debye–Scherer's equation[15] as revealed as following:

$$t = \frac{0.89\lambda}{\beta_{hkl}\cos\theta_{hkl}}$$

147   (2)

148   where t is the crystallite size for (hkl) phase (nm), l is the X-ray wavelength of radiation for

149   CuKα, β_{hkl} is the full width at half maximum (FWHM) at (hkl) peak in radian and θ is the

150   diffraction angle for (hkl) phase.

151   The specific surface area, average pore size total pore volume and pore size

152   distribution of the $Ca(OCH_3)_2$ catalysts were determined from the corresponding nitrogen

153   adsorption-desorption isotherms at liquid nitrogen temperature (-196 ^{o}C) with a Thermo

154   Finnigan Sorptomatic 1900 series. The isotherms were generated by dosing nitrogen onto the

155   catalyst. Before adsorption measurements, all the catalysts (0.5 g) were degassed for 8 h at

156   150 °C under vacuum circumstance until pressure gradient reach an extremely low state. The

157   total surface area (S_{BET}), total pore volume (cm^3 g^{-1}) and average pore size (nm) of the

158   catalysts was generated from adsorption-desorption isotherms by using the Brunauer–

159   Emmett–Teller (BET) method. Whereas, the pore size distribution was evaluated from

160   desorption branches by using Barrett–Joyner–Halenda (BJH) plot.

161   Infrared spectra of solid $Ca(OCH_3)_2$ catalysts were measured by using attenuated total

162   reflection-Fourier transform-infrared (ATR-FTIR) on a Perkin Elmer (PC) Spectrum 100

163   FTIR spectrometer to identify the surface functional groups presenting on the catalyst at

164   room temperature. Each spectrum was average of 128 scans analysed over the scanning over

165   a wavelength of 650 – 4000 cm^{-1} at a resolution of 4 cm^{-1}.

166   The morphological observations of the prepared $Ca(OCH_3)_2$ catalysts were made by

167   Field Emission Scanning Electron Microscopy (FESEM, JOEL, JSM-6700F) and

168   Transmission Electron Microscopy (TEM, Hitachi, H7100). For FESEM analysis, the

169   catalysts were coated with Au (gold) for protecting the induction of electric current using a

170   Sputter Coater. Whereas, particle size of the $Ca(OCH_3)_2$ catalysts were obtained by using

171   TEM with an accelerating voltage of 200 kV.

172
173   **Methanolysis of triglycerides**

174   Production of biodiesel by methanolysis of crude *J. curcus* derived oil, over $Ca(OCH_3)_2$

175   catalyst, was performed using a 100 ml two-neck round bottom flask equipped with a water-

176   cooled reflux condenser and continuous stir at 900 rpm. The reaction allowed proceeding in

177   a controlled temperature of silicon oil bath in order to keep the temperature constant.

178   Typically, CMX (X= 2-12) catalyst was suspended in a required volume (n(methanol):n(oil) =

179   12:1) of methanol. The reaction temperature was controlled at 65 ^{o}C by a silicon oil bath.

180   Consequently, crude JCO (10 g) was added into the mixture under vigorous stirring in the

181   presence of catalyst (2 wt. %). Once the reaction had finished (1.5 h), the mixture was then

182   cooled to room temperature. After cooling, the catalyst was separated via centrifugation and

183   the residual methanol and glycerol of the by-product were eliminated by washing with water.

184   The transesterified oil was collected after the separating process mentioned above, and was

185   dried with help of a rotary evaporator under reduced pressure prior to analysis.

186
187   **Analysis of fatty acid methyl esters**

188   The yield of FAME produced was carried out using a gas chromatography on Shimazu GC-

189   14C. Split type injector and a flame ionization detector (FID) were connected to a polar BP-

190   20 capillary column (30 m × 0.5 mm × 0.25 μm). The transesterified oil was injected at 140

191   °C with the split ratio of 1:30. FAME was separated from the transesterified oil in the column

192   heated at 250 °C with the heating rate at 5 °C /min. Methyl heptadecanoate was used as an

193   internal standard and dichloromethane was used as a solvent. The FAME content was

194   determined in agreement with European regulated procedure EN 14103.[16] FAME content (%)

195   was calculated using the equations as following:

196
197   FAME yield (%) = [(m_{FAME} / MW_{FAME}) x C_{FAME}] / [(m_{JCO} / MW_{JCO}) x 3]   × 100 %   (3)

198   where m_{FAME} and m_{JCO} are the mass of FAME produced and JCO, respectively. Furthermore,

199   MW_{FAME} and MW_{JCO} are the average molecular weights of FAME produced and JCO,

200   respectively, which were calculated according to the composition of fatty acids.

201 Additionally, C_{FAME} is the FAME concentration. "3" represented the coefficient

202 present in equation whereby it descript for the fact that each triglyceride molecule yields

203 three methyl ester molecules.

204
205 **Recyclability study of produced catalyst**

206 To study the catalyst lifetime and stability, the used CM8 catalyst was separated from

207 reaction mixture and reuse in transesterification reaction without additional treatment. In this

208 case, crude JCO and methanol were added in the same amount into each reaction system, and

209 the reactions were performed at the optimum condition.

210
211 **RESULTS AND DISCUSSION**

212 **Properties of crude *Jatropha curcas* L. oil**

213 The crude JCO was found contain 0.091 % w/w of moisture. Other analyses for the crude

214 JCO were density value of 0.9162 g/cm^3, saponification value of 188.4 m_{KOH}/m_{oil}, mg/g and

215 acid value of 13.6 m_{KOH}/m_{oil}, mg/g, respectively. Therefore, average molecular weight of *J.*

216 *curcus* oil was calculated as 962.8 g/mol. Since the content of free fatty acids is 6.8 % w/w

217 which in the higher range.

218 The gas chromatography results showed that FAME constituents present in *J. curcus*

219 oil were methyl palmitate ($C_{16:0}$), methyl palmitoleate ($C_{16:1}$), methyl stearate ($C_{18:0}$), methyl

220 oleate ($C_{18:1}$), methyl linoleate ($C_{18:2}$) and methyl arachidate ($C_{20:0}$), whereby, unsaturated

221 methyl ester is the most prominent compound.

222 The methyl ester composition of crude JCO is shown in Table 1, which consisting

223 72.4 % of unsaturated fatty acids (USFA), whereas the level of saturated fatty acid (SFA) was

224 27.6 %. This outcome has a well conformation with the profiles in literatures.[10] The GC data

225 of other biodiesel fuels revealed the fatty acid profiles were comparative to the major

226 constituent of ester derived from crude JCO. However, crude JCO exhibited the high

227 unsaturated/saturated lipid ratio with the sequence soybean methyl esters (SBME) > crude

228 *Jatropha curcus* oil methyl esters (CJCOME) > *Citrus reticulate* methyl esters (CiRME) >

229 palm oil methyl esters (POME) > sunflower oil methyl esters (SFOME).

230
231 **Catalyst characterization**

232   In thermogravimetric analysis (TGA), the weight of synthesized catalyst was

233 measured as the function of temperature while it was subjected to a controlled heating

234 programme. The amount of weight loss provided a quantitative indication about the

235 composition of catalyst. Additionally, temperature of thermal and oxidative degradation of

236 catalyst was also measured using differential thermal analysis (DTA). The curve showed the

237 physical and chemical transitions of the sample by measuring exothermic and endothermic

238 effects.

239   Fig. 1 corresponds to the TG/ DTA thermogram of synthesized $Ca(OCH_3)_2$ catalyst

240 under air flow condition. The TGA curve remained constant from 35 °C to 370 °C.

241 $Ca(OCH_3)_2$ catalyst begins to decompose at about 370 °C with weight loss of around 17 %.

242 This phenomenon was due to a chemical reaction occurred. The DTA curve shows an

243 exothermic peak appears between 370 and 460 °C which consistent with peak at TGA curve.

244 The reaction at 430 °C might result in the decomposition of $Ca(OCH_3)_2$ with oxygen to

245 calcium carbonate as following (Scheme 3):

246
247      $$Ca(OCH_3)_2 + 3O_2 \longrightarrow CaCO_3 + CO_2\uparrow + 3H_2O\uparrow \quad \text{(exothermic)}$$

248
249 Furthermore, the TGA curve had evidenced thermal decomposition of calcium carbonate with

250 the formation of gaseous products after 600 °C. A steep slope was observed between 600 and

251 800 °C from TGA curve. At 720 °C, the DTA peak showed endothermic transformation of

252 $CaCO_3$ to stable CaO. The thermogravimetry analysis suggested that the synthesized

253     $Ca(OCH_3)_2$ catalyst is stable below 400 °C. Thus, the produced $Ca(OCH_3)_2$ catalyst is

254   extremely stable during transesterification reaction.

255   The XRD patterns of all the catalysts are shown in Fig. 2 CaO given very appreciable

256   broad peaks at 2θ of 32.1° and 37.2° (JPDS File No. 00-037-1497). $Ca(OCH_3)_2$ was

257   characterised with the presence peak at 2θ of 10.8°[17] for CM2 - CM12 catalysts.. The

258   insignificant three peaks at 2θ of 17.8°, 28.6°, and 34.0° were suggested the existence of

259   calcium hydroxide (JCPDS file No: 01-84-1264) which has probable appeared due to the

260   interaction of catalyst with the water molecules formed as a byproduct during the synthesis

261   reaction.

262   The crystallite size and surface area of the catalysts were summarized in Table 2. As

263   can see, the average crystallite size for pure CaO catalyst was 66.3 nm. All the catalysts were

264   showed the metal methoxide particles with 29.0, 31.1, 30.6, 27.5, 29.7 and 31.4 nm in

265   crystallite sizes. These results indicated that particle sizes of the final products were being

266   reduced significantly to become 2 times smaller compare to pure metal oxide clusters. The

267   results also showed that crystal sizes of catalysts were in agreement with the line width of the

268   peak in which decrease of FWHM with the increment of the crystallite size.

269   The surface areas of all the catalysts are shown in Table 2. The surface area of the

270   catalysts was in agreement with XRD analysis which showed that lower the crystallite sizes

271   gave higher surface area as demonstrated in Fig. 3. BET isotherm of CM8 catalyst which

272   resembles the Type IV isotherms with hysteresis loop of type H3 based on IU-PAC

273   classification.[18,19] The measured surface area, total pore volume and average pore diameter of

274     $30.5 \text{ m}^2\text{g}^{-1}$, $0.21 \text{ cm}^3\text{g}^{-1}$ and 31.97 nm, respectively. Therefore, this was suggested the catalyst

275   was favourable to be used in the liquid phase reaction since it can provide sufficient large

276   area of active site in stirrer type reactor.[20]

277   The pore size distribution of CM8 catalyst reveals the surface is occupied by

278   relatively small size of mesopore structure range of 2 to 5 nm shown in Fig. 4. Mesoporous

279   materials can serve as effective catalysts in transesterification reactions for adsorbing large

280   organic molecules due to uniform pore structure and extensively high surface area.

281   Furthermore, a large part of surface was fully occupied by larger pore structure with size

282   between 6 to 100 nm. The macropore structure of the particle catalyst provides rapid mass

283   transfer into the interstices of the catalyst and lead reagent to the ultimate reaction sites.

284   Consequently, high surface area and porosity properties are important characterizations of

285   solid catalyst because they are closely related with the catalytic activity.

286   FTIR spectrum of synthesized $Ca(OCH_3)_2$ catalysts at room temperature were showed

287   in Fig. 5, which indicated that the important features appear in the -C-O stretching vibration

288   of primary alcohol (1070 cm^{-1}), -OH stretching vibration of primary alcohol (3650 cm^{-1}),

289   CH_3 stretching vibrations (2800–3000 cm^{-1}) and -C-H alkene bending (1465 cm^{-1}).[20,21]

290   Furthermore, it was found the unusual peak appeared at 3650 cm^{-1} suggested to the

291   adsorption of water on the surface of all catalysts. This peak indicates the existence of -OH

292   functional groups isolated on calcium cation.[20] Since water was produced as a by-product in

293   the catalyst synthesis reaction, these isolated -OH groups might have produced from water

294   facilitated by the strong basic property of $Ca(OCH_3)_2$ catalyst as shown as (Scheme 3).

295   The particle morphology of all the catalysts is summarized in Table 2. It was found

296   that the difference of synthesis time leads to the different morphologies of $Ca(OCH_3)_2$

297   catalyst as shown in TEM (Fig. 6) and FESEM (Fig. 7) images. Fig. 6(a) and 6(b) shows the

298   TEM images of parent and non-modified CaO as starting material. The TEM images of CaO

299   showed a cluster of well-developed cubic crystal. The particle sizes were measured from the

300   TEM image and average particle sizes were 137.02 ± 11.30 nm in diameter. Structure of

301   commercial CaO catalyst showed surface unevenness (Fig. 7(a) and 7(b)).

302   Fig. 6(c) and 6(d) shows TEM images of CM2 catalysts synthesized with 2 hours,

303 giving cubic crystal of CaO and irregular round shaped $Ca(OCH_3)_2$ with 170.71 ± 25.26 nm

304 and 68.06 ± 19.29 nm in diameter, respectively. Increasing the synthesis time of showed no

305 significant changing in morphology was found on CM4 catalyst (Fig. 6(e) and 6(f)).

306 However, TEM images revealed the average particle sizes measurement were reduced to

307 120.07 ± 23.32 nm and 34.74 ± 3.26 nm in diameter. The shape of CM2 and CM4 catalysts

308 were confirmed by FESEM as shown in Fig. 7(c), 7(d), 7(e) and 7(f). These results are

309 consistent with the results obtained, corroborating conclusion extracted from XRD patterns

310 about the existence of CaO and $Ca(OCH_3)_2$ particles.

311   On the other hand, Fig. 6(g) and 6(h) demonstrated the TEM photos of CM6 catalyst

312 composed of bundles of biconvex like structure particles (view from top of plate-like shape

313 particles). The average particle sizes of CM6 as determined from TEM images show its

314 diameter and thickness of 267.10 ± 35.10 nm and 72.46 ± 22.34 nm, respectively.

315 Furthermore, a small amount of well arrange irregular plate-like shape particles is clearly

316 visible on the external surface of catalyst observed in Fig. 7(g) and 7(h). A minute amount of

317 particles or patches also coexisted. A close-up view of Fig. 7(g) and 7(h), showed a typical

318 plate like structure with overall size of about 70 nm in length, and a few small particles

319 attached on the assembled plates formed rough surface particles. This result is consistent with

320 the result gained from morphological studies by FESEM technique.

321   A representative TEM images of CM8 catalyst displayed in Fig. 6(i) and 6(j). From

322 the magnified TEM image in the inset, the featured of rigid biconvex like structure particles

323 were sufficiently revealed by appearances of the clear edge (Fig. 6(j)). The averages sizes of

324 CM8 determined from TEM images (Fig. 6(i) and 6(j)) were 391.77 ± 65.34 nm in diameter

325 and 111.38 ± 13.12 nm in length, correspondingly. The primary particles of CM8 catalyst

326 were appeared to be formed abundant cluster of thin plates shown in Fig. 7(i) and 7(j).

327   Increasing the synthesis time not only resulted in the high quantities and uniform morphology

328   but also enhanced a large number of pores which are visible on the surface of the catalyst.

329   The pores and thin plate-like morphology was contributed to the high surface area of catalyst.

330   The close-up view in the inset of Fig. 7(j) showed the thin plate particles possessed a smooth

331   surface state with the size about 100 nm in length, almost consistent with FESEM

332   observations.

333   Fig. 6(k) and 6(l) showed TEM photos of CM10 catalyst consisting of aggregated

334   biconvex like structure particles (530.41 ± 21.69 nm in diameter and 157.38 ± 5.69 nm in

335   thickness) and large aggregated round particles (302.30 ± 46.93 nm in diameter). The higher

336   crystallinity of CM10 is confirmed by FESEM (Fig. 7(k) and 7(l)). The crystallites of CM10

337   catalyst are larger than those observed for CM8 catalyst, which presents aggregates of

338   variable morphology. The monograph of FESEM endorsed the crystallinity result of XRD.

339   TEM micrographs of CM12 catalyst gave irregular shape of $Ca(OCH_3)_2$ when pro-

340   long the synthesis time to12 hours. The particle sizes were measured from the TEM image

341   and average particle sizes were 366.52 ± 24.82 nm in diameter as shown in Fig. 6(m) and

342   6(n). FESEM micrographs of CM12 catalyst gave irregular bulky round-shape on the external

343   surface of catalyst as shown in Fig. 7(m) and 7(n). The CM12 catalyst with compact

344   agglomeration was in agreement with TEM images.

345   The results demonstrated that the duration of the synthesis time is the key for

346   controlling the morphology evolution of the cluster thin plate-like calcium methoxide

347   architectures. The collapsing of the plate-like structure of calcium methoxide catalysts was

348   lead to the reduction of total surface area of the catalysts. Notice that from Table 2, the

349   particle sizes measured between XRD and TEM show dissimilarity. The sizes obtained from

350   TEM were greater than that obtained from the XRD measurement. This deviation is known to

351   depend on the aspect ratio for nonplated shaped crystallites, apart from the contributions to

352   the FWHM by the microstrain in the crystallite.[22] Despite this limitation the agreement that is

353   seen between the sizes measured by these two techniques may be taken to be good in terms of

354   the conclusion drawn on the shape and to a limited extent on the approximate true size of

355   these crystallites.

356

357   **Transesterification reaction: correlation between biodiesel yield with synthesis time,**

358   **surface area and morphology of catalysts**

359   Transesterification reaction involved the cleavage of ester group RCOO⁻, from triglycerides

360   (TG), by an alcohol moiety of methanol to produce new esters with original alcohol moiety

361   exchanged with the reacting alcohol. Since there are three ester groups of a TG molecule, the

362   three fatty acid moieties are attached to a single alcohol moiety yielded intermediate

363   formation of diglycerides (DG), monoglycerides (MG) and glyceride (Gly). The consecutive-

364   competitive steps of transesterification reaction between TG and methanol are shown in

365   Scheme 4.

366
367

368

369
370

15
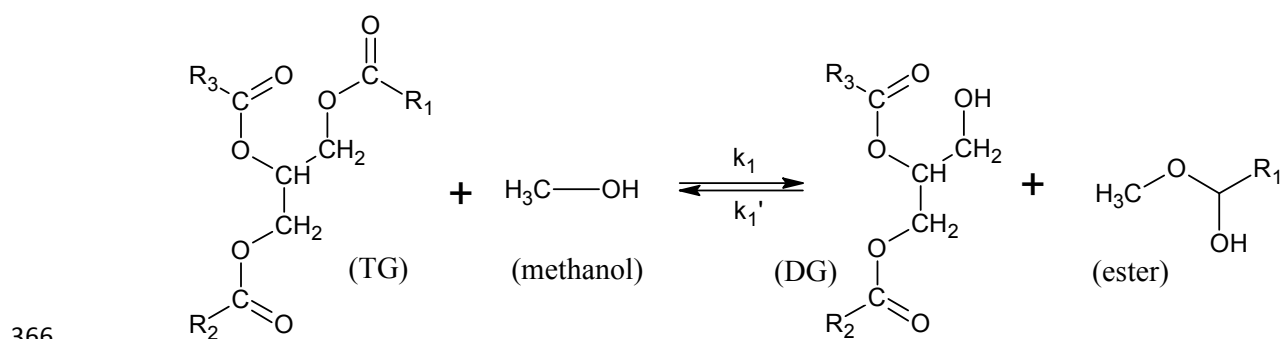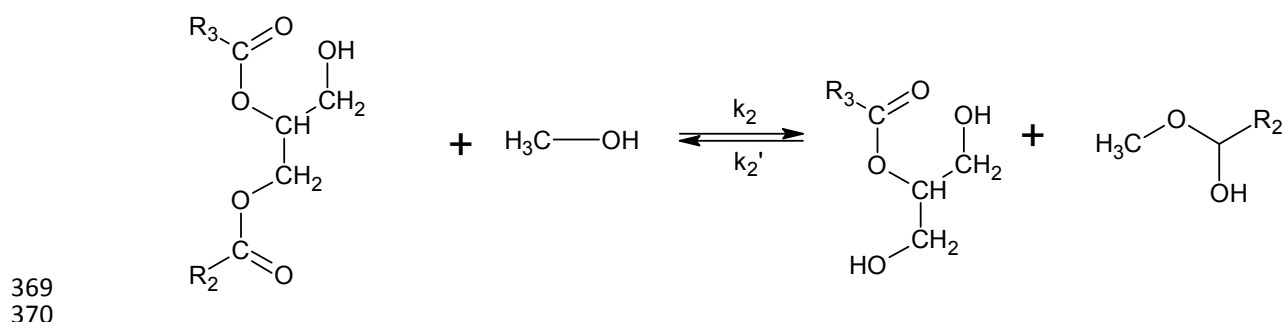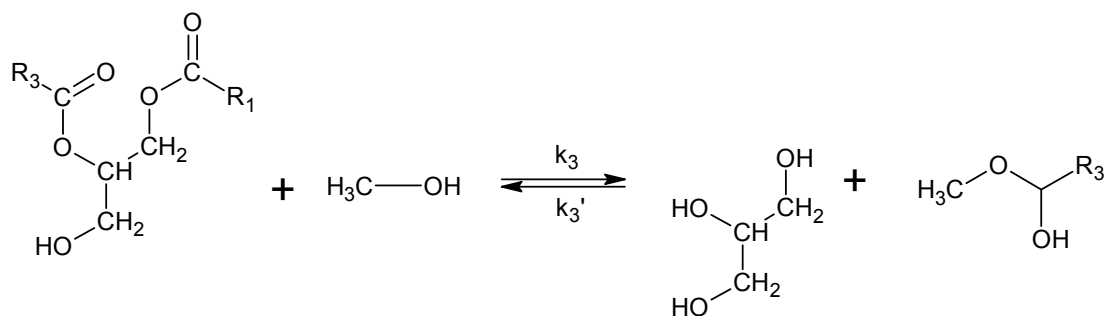
Where, R_1, R_2 and R_3 are the alkyl group

Scheme 4 Stepwise consecutive transesterification reaction and formation of DG, MG and Gly.

Different synthesis times of bulk $Ca(OCH_3)_2$ catalysts on transesterification of crude JCO is presented in Table 3. It is noteworthy that the catalytic activity of synthesized $Ca(OCH_3)_2$ catalysts showed high transesterification activity in the range of 74 – 87 % under condition of: 2 wt. % of catalyst, molar ratio of methanol /oil (12:1) and reaction time 2 h at 60 ^{o}C. The FAME yield was increased from CM2 to CM8, while further increment of synthesis time from CM10 to CM12 resulted in small decreases in catalytic performance.

BET surface area of catalyst is believed to be an important factor which affect on the catalytic activity,[12,20,23] the correlation between surface area of catalysts and FAME yield is demonstrated in Fig. 8. The enhance in FAME content from 74 – 87 % while shifting from CM2 to CM8 might be due to the increase of catalysts' surface area from 16.2 – 30.5 m^2g^{-1}. Further increment of synthesis time from CM10 to CM12 lead to slightly drop of surface area with 28.8 and 26.0 m^2g^{-1}, respectively. The collapsing plate-like structures at CM10 and CM10 tend to reduced catalyst's surface area. Lower catalysts' surface for synthesis time above 8 h is the reason contributed to the decrease of catalyst activity. This might due to the diffusion limitation between the reactant and the active sites which were located inside the pores of the catalyst.

As shown in Fig. 8, morphology of CM2 and CM4 catalysts revealed to be irregular round shape with surface area lower than CM8 catalyst. However, the catalytic activity was

16

394 comparative among them. This probably due to the synergetic effect of the presence of CaO

395 and $Ca(OCH_3)_2$ phases in CM2 and CM4 catalysts that observed from XRD profile (Fig. 2).

396 Lower surface area of CM2 and CM4 catalysts was contributed by CaO phases. Excessive

397 CaO phases caused lesser porosity on catalyst surface, which contribute to the reduction in

398 surface area. On the other hand, BET surface area of CM6 was 20.5 m^2g^{-1} gave raised the

399 FAME yield at 81.2 %. The present of well arrange irregular plate-like shape particles in

400 catalyst provided more active surface for tranesterification reaction.

401   Obviously, CM8 catalyst was exhibited much higher biodiesel production than that of

402 other catalysts, and a biodiesel yield of 87.1 % is achieved at 2 h. There was only pure

403 $Ca(OCH_3)_2$ site found at CM8 catalyst to be the highest surface area which provide strong

404 basic property toward the transesterification reaction. The cluster thin plate-like architectures

405 of CM8 catalyst showed mesoporous and macroporous properties of catalyst as shown in Fig.

406 4. Mesoporous and macroporous materials can serve as effective catalysts in

407 transesterification reactions for adsorbing large organic molecules to uniform structure and

408 extensively high surface area.[12,20] Therefore, the reactivity of a catalyst is directly correlated

409 with the external surface area of the catalyst.
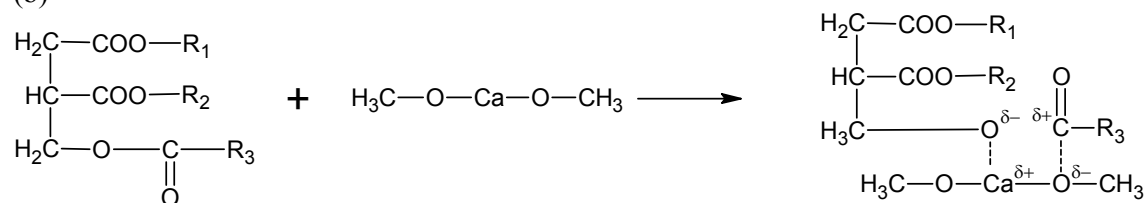
410
411 **Recyclability study**

412 Fig. 9 summarizes the experimental results of reusability between $Ca(OCH_3)_2$ and CaO

413 catalysts. Unlike CaO catalyst, the transesterifying operation of $Ca(OCH_3)_2$ catalyst was

414 successively repeated 5 times and maintained sustained activity to produce yield in excess 86

415 % biodiesel at 65 °C. The biodiesel yield was only slightly reduced at the following uses.

416 Due to less porosity and active surface basic sites of CaO catalyst, it was not favors for

417 transesterification of crude JCO at short reaction time in the presence of only low

418 concentration of catalyst[23].

419   The proposed mechanism of the transesterification reaction by Ca(OCH$_3$)$_2$ catalyst

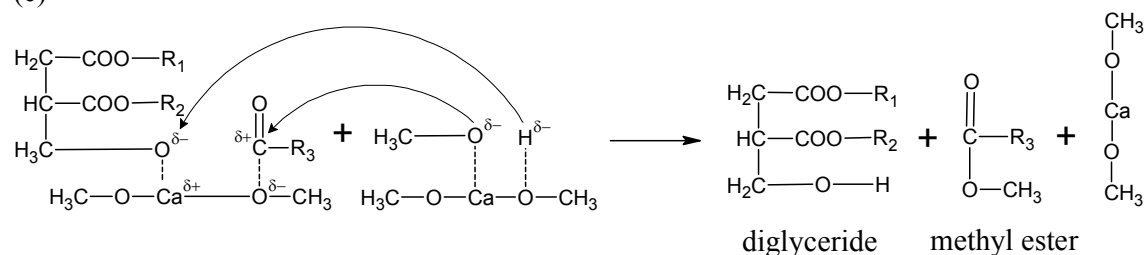420   with methanol and triglyceride process is demonstrated in Scheme 5.

421   (a)

$$O^{\delta-}\!-\!CH_3$$

$$H_3C-O-Ca-O-CH_3 \quad + \quad H_3CO-H \longrightarrow H_3C-O-Ca-O-CH_3$$

          calcium methoxide   methanol $\overset{\delta+}{H}$

422

423   (b)

H$_2$C—COO—R$_1$ H$_2$C—COO—R$_1$

HC—COO—R$_2$ +   H$_3$C—O—Ca—O—CH$_3$ ⟶   HC—COO—R$_2$

H$_2$C—O—C—R$_3$ $H_3C \underset{\delta-}{\quad\quad} O^{\delta-} \overset{\delta+}{C}-R_3$

            ‖ $H_3C-O-Ca^{\delta+}\!-\!O^{\delta-}\!-\!CH_3$

            O

424

425   (c)

H$_2$C—COO—R$_1$ CH$_3$

HC—COO—R$_2$ H$_2$C—COO—R$_1$ O |

$H_3C \quad O^{\delta-} \overset{\delta+}{C}-R_3$ + $H_3C-O^{\delta-} H^{\delta-}$ ⟶ HC—COO—R$_2$ + $\overset{\parallel}{C}-R_3$ + Ca

$H_3C-O-Ca^{\delta+}\!-\!O^{\delta-}\!-\!CH_3$ $H_3C-O-Ca-O-CH_3$ H$_2$C—O—H   O—CH$_3$ CH$_3$

426

                                                   diglyceride   methyl ester
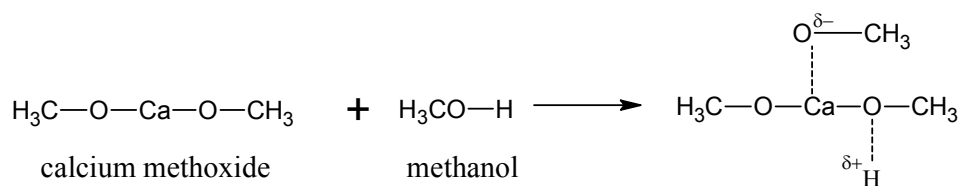
427

428   **Scheme 5** Reaction mechanism for the transesterification of triglyceride with methanol over

429   the calcium methoxide catalyst, where R$_1$, R$_2$ and R$_3$ represent the long chain alkyl group.

430

431   Firstly, when calcium methoxide is used as a solid base catalyst, the catalysis

432   mechanism could be assumed that the catalytic reactions take place on the surface of catalyst

433   with Ca$^{\delta+}$ and O$^{\delta-}$ being the two catalytic active sites participating in the reaction. Methanol

434   and triglyceride are adsorbed on the two neighboring free catalytic site as indicated by step

435   (a) and step (b). In step (a), the surface O$^{\delta-}$ is extracted H$^{\delta+}$ and Ca$^{\delta+}$ adsorbed CH$_3$O$^{\delta-}$ from

436   methanol. Meanwhile, the adsorbed triglyceride forms a surface intermediate between O$^{\delta-}$

437   with the Ca$^{\delta+}$ on the surface of the catalyst is shown in step (b). The two neighboring

438   adsorbed species react with each other, in step (c), which results to the formation of a fatty

439   acid methyl ester and a diglyceride. Using the stepwise consecutive and reversible raction,

440   the diglyceride and monoglyceride are reacts with methanol on the surface of catalyst to

441   prodece methyl esters and glycerol in a similar fashion.

442
443   **CONCLUSIONS**

444    $Ca(OCH_3)_2$ is a powerful heterogeneous catalyst for transesterification reaction of non-edible

445   *Jatropha curcas* oil for biodiesel production. $Ca(OCH_3)_2$ catalysts gave raised three types of

446   morphologies such as irregular round shape particles, a well arrangement of plate-like

447   structures with rough surface and a cluster of tiny plate-like architectures with smooth

448   surface. Under optimum condition of 60 $^{\circ}$C, 12:1 methanol to oil molar ratio and 2 % catalyst

449   concentration, above 87 % yield was achieved in 2 h. $Ca(OCH_3)_2$ catalyst can be separated

450   easily from the reaction mixture and reused to give a consistent transesterification activity

451   (five times reuse). Hydrothermal method is simple and easy operation steps to fabricate

452    $Ca(OCH_3)_2$ catalyst. The produced $Ca(OCH_3)_2$ catalyst can be used for transesterification of

453   trimethylolpropane to bio-lubricant production, ring-opening polymerization of lactone and

454   effective consolidants precursor material for polymerization.

455
456   **Notes and references**

457   1 M. Kouzu and J. S. Hidaka, *Fuel*, 2011, 93, 1.

458   2 U. Rashid, I. I. Muhammad, Y. Shahid, Y. Robiah and Y.H. Taufiq-Yap, *Ind. Crop. Prod.*,

459   2013, 45, 355.

460   3 C. Ngamcharussrivichai, P. Totarat and K. Bunyakiat, *Appl. Catal. A*, 2008, 341, 77.

461   4 Y.H. Taufiq-Yap, H.V. Lee, M.Z. Hussein and R. Yunus, *Biomass Bioenerg.*, 2011, 35,

462   827.

463   5 H. Kabashima, H. Tsuji and H. Hattori, *Appl. Catal. A*, 1997, 165, 319.

464   6 M.L. Granados, D.M. Alonso, I. Sadaba, R. Mariscal and P. Ocon, *Appl. Catal. B*, 2009,

465   89(1-2), 265.

466   7 M.S. Jin, Q. Kuang, Z.Y. Jiang, T. Xu, Z.X. Xie and L.S. Zheng, *J. Solid State Chem.*,

467   2008, 181, 2359.

468   8 B. Cheng and E. T. Samulski, *Chem. Commun*, 2004, 8, 986.

469   9 J. M. Jang, C.R. Kim, H. Ryu, M. Razeghi and W.G. Jung, *J. Alloy and Compd.*, 2008, 463,

470   503.

471   10 Y. Arai and Y. Wakui, *Nikka*, 1981, 9, 1402.

472   11 S. Gryglewicz, *Bioresour. Technol.,* 1999, 70, 249.

473   12 X. Liu, X. Piao, Y. Wang and S. Zhu, *Fuel*, 2008, 22(2), 1313.

474   13 F. Liu and Y. Zhang, *Ceram. Int.*, 2011, 37, 3193.

475   14 K. F. Yee, J. C. S. Wu and K. T. Lee, *Biomass Bioenerg.*, 2011, 35, 1739.

476   15 B. D. Cullity, Addison-Wesley, 1978, London.

477   16 A. Islam, Y.H. Taufiq-Yap, C.H. Chu, P. Ravindra, and E.S. Chan, *Renew. Energ.*, 2013,

478   59, 23.

479   17 H. P. Zhu, Z. B. Wu, Y. X. Chen, P. Zhang and S. J. Duan. *Chin. J. Catal.*, 2006, 27, 391.

480   18 V. G. Deshmane and Y.G. Adewuyi, *Fuel*, 2013, 107, 474.

481   19 K.S.W. Sing, D.H. Everett, R. A. W. Haul, L. Moscou, R. A. Pierotti and J. Rouquerol,

482   *Pure Appl. Chem.,* 1985, 57, 603.

483   20 M. Hassan, Y. Robiah, S.Y.C. Thomas, U. Rashid and Y.H. Taufiq-Yap. *Appl. Catal. A*,

484   2012, 425-426, 184.

485   21 M. Kouzu, J.S. Hidaka, K. Wakabayashi and M. Tsunomori, *Appl. Catal. A*, 2010, 390,

486   11.

487   22 D. Sarkar, S. Tikku, V. Thapar, R.S. Srinivasa and K. C. Khilar. *Colloids Surf. A*, 2011,

488   381, 123.

489   23 S. H. Teo, U. Rashid, Y. H. Taufiq-Yap, *RSC Adv.*, 2014, 4, 48836.

490

491 Table 1 Fatty acid composition of crude *Jatropha* oil- based methyl esters (CJCOME) with
492 comparison to other esters using GC-FID analysis
493

FAMEs	Carbon	[a] CJCOME	[b] POME	[c] CiRME	[d] SBME	[e] SFOME
Lauric acid	12:0	-	0.9	-	-	-
Myristic acid	14:0	-	1.5	-	-	-
Palmitic acid	16:0	20.2	41.9	26.9	12.5	46.0
Palmitoleic acid	16:1	1.1	-	-	-	-
Stearic acid	18:0	7.2	2.7	4.6	5.2	4.0
Oleic acid	18:1	39.8	40.8	25.6	23.5	40.0
Asclepic	18:1 (n-7)	-	-	1.2	-	-
Linoleic acid	18:2	31.2	11.9	37.7	48.8	10.0
Linolenic acid	18:3	0.3	0.3	3.8	10.0	-
Arachidic acid	20:0`	0.2	-	0.2	-	-
[d] $\sum_{SFA}$		27.6	47.0	31.7	17.7	50.0
[e] $\sum_{USFA}$		72.4	53.0	68.3	82.3	50.0

494 [a] CJCOME (Crude *Jatropha curcus* oil methyl esters); [b] POME (Palm oil methyl esters) [21]; [c] CiRME (*Citrus*
495 *reticulate* methyl esters) [2]; [d] SBME (Soybean methyl esters) [11]; [e] SFOME (Sunflower oil methyl esters) [2].
496 [d] Total saturated fatty acid
497 [e] Total unsaturated fatty acid
498
499
500
501
502
503
504
505
506
507
508
509
510
511
512
513
514
515
516
517
518
519

520   Table 2 Crystallites sizes, BET surface area, shape and particle size of calcium methoxide
521   catalysts.
522

Catalyst	2θ (^{o})	FWHM	[a]Crystalitite size (nm)	[b]S_{BET} (m^2g^{-1})	[c]Shape	[c]Particle size (nm)
CaO	37.4701	0.1510	66.3	9.2	Cubic crystal	137.02 ± 11.30
CM2	10.8448	0.2784	29.0	16.2	Cubic crystal + irregular round	170.71 ± 25.26 & 68.06 ± 19.29
CM4	10.8348	0.2597	31.1	18.3	Cubic crystal + irregular round	120.07 ± 23.32 & 34.74 ± 3.26
CM6	10.8248	0.3074	30.6	20.5	Plate	267.10 ± 35.10 (D) 72.46 ± 22.34 (T)
CM8	10.8105	0.2941	27.5	30.5	plate	391.77 ± 65.34 (D) 111.38 ± 13.12 (T)
CM10	10.8213	0.2721	29.7	28.8	Plate + round	530.41 ± 21.69 (D) 157.38 ± 5.69 (T) & 302.30 ± 46.93
CM12	10.8223	0.2847	31.4	26.0	Irregular bulky round	366.52 ± 24.82

523   [a] Determined from XRD patterns using Sherrer's equation.
524   [b] BET surface area.
525   [c] Observed by TEM analysis.
526   [d] Measured by SEM techique.
527
528
529
530
531
532
533
534
535
536
537
538
539
540
541
542
543
544
545
546
547
548
549
550
551
552
553
554
555
556
557

558 Table 3 Transesterification activities of bulk CM2, CM4, CM6, CM8, CM10 and CM12
559 catalysts with different synthesis times for biodiesel production[a]
560

Catalysts	Yield of FAME (%)
CM2	74
CM4	78
CM6	81
CM8	87
CM10	79
CM12	80

561 [a] Transesterification condition: catalyst dosage 2 %, n(methanol):n(JCO) =12:1, reaction time   2 h, reaction
562 temperature 65 °C.
563
564

1
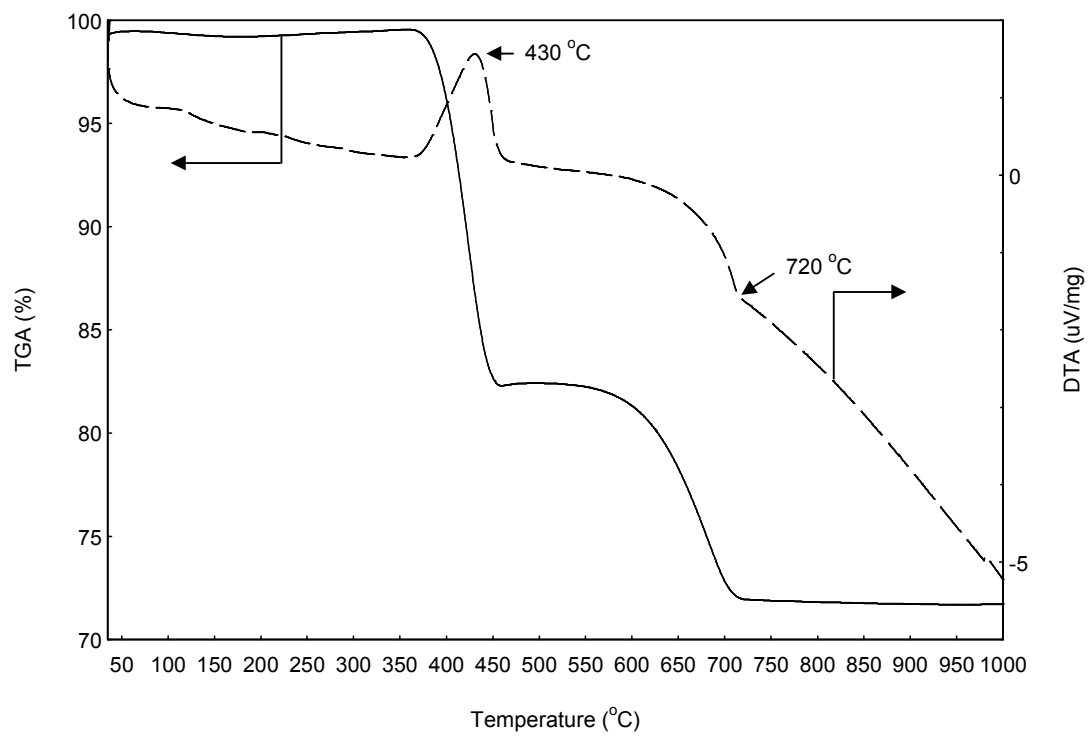
2

3   Fig. 1 TG/DTA spectrum of calcium methoxide catalyst.

4

5

6

7

8

9

10

11

12

13

14

15

16

17
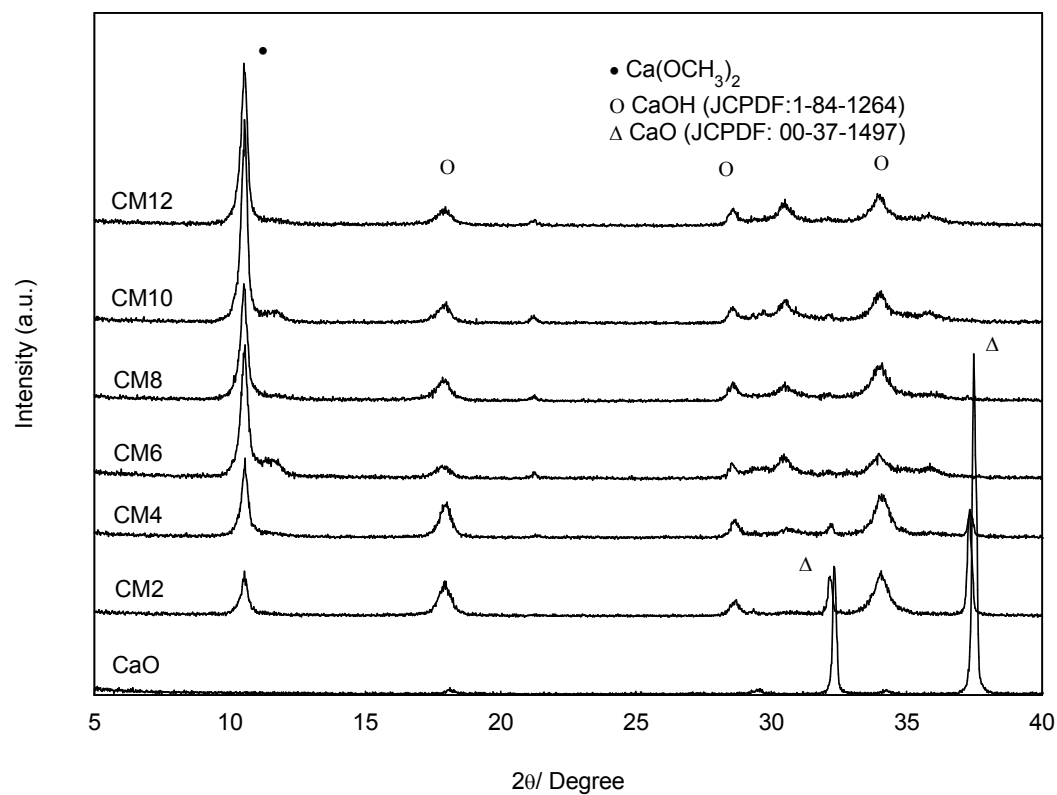
Fig. 2 X-ray diffraction patterns of calcium oxide and calcium methoxide catalysts. $Ca(OCH_3)_2$ prepared with methanol reflux of CaO at 65 ^{o}C (under 50 ml/min nitrogen flow condition) for 2, 4, 6, 8, 10 and 12 hours which hence labeled as CM2, CM4, CM6, CM8, CM10 and CM12. ●, characteristic peak of calcium methoxide; Δ, characteristic peak of calcium oxide; ○, characteristic peak of calcium hydroxide.
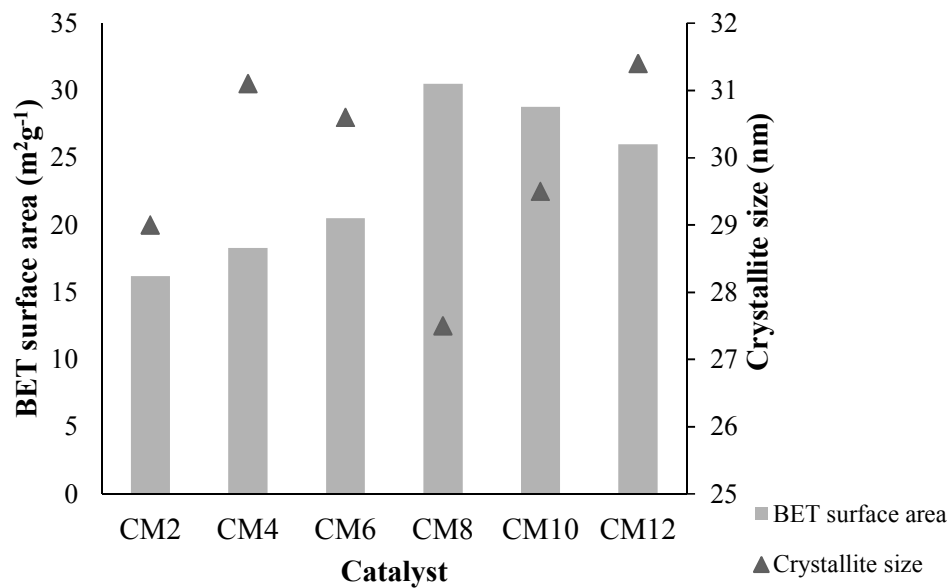
Fig. 3 Crystallites sizes and BET surface area and calcium methoxide catalysts.
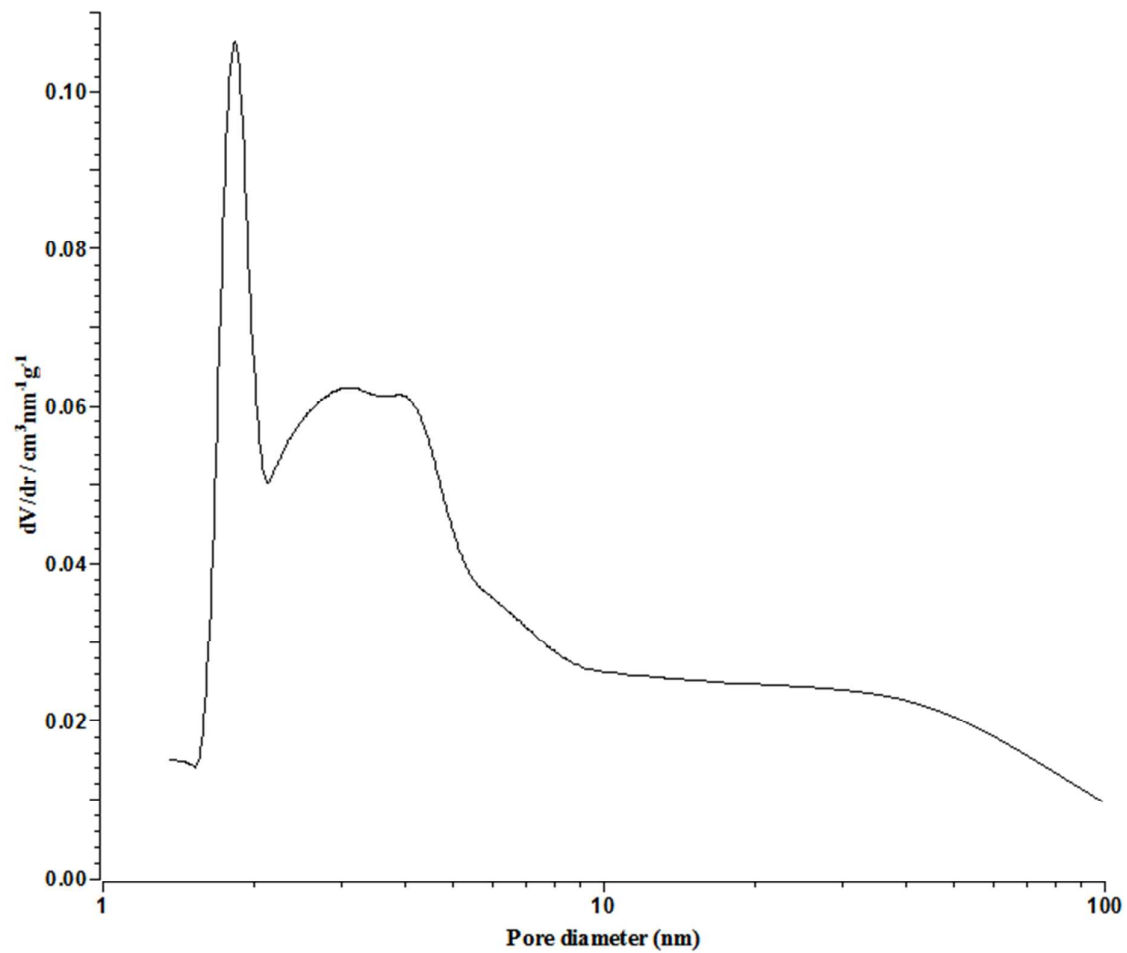
Fig. 4 Pore size distribution of calcium methoxide catalyst.

CM2

CM4

CM6

CM8

CM10

Transmittance (%)

CM12

(d) 3650 cm^{-1}

(b) 1465 cm^{-1}

(c) 2800-3000 cm^{-1}

(a) 1070 cm^{-1}

Wavenumber (cm^{-1})
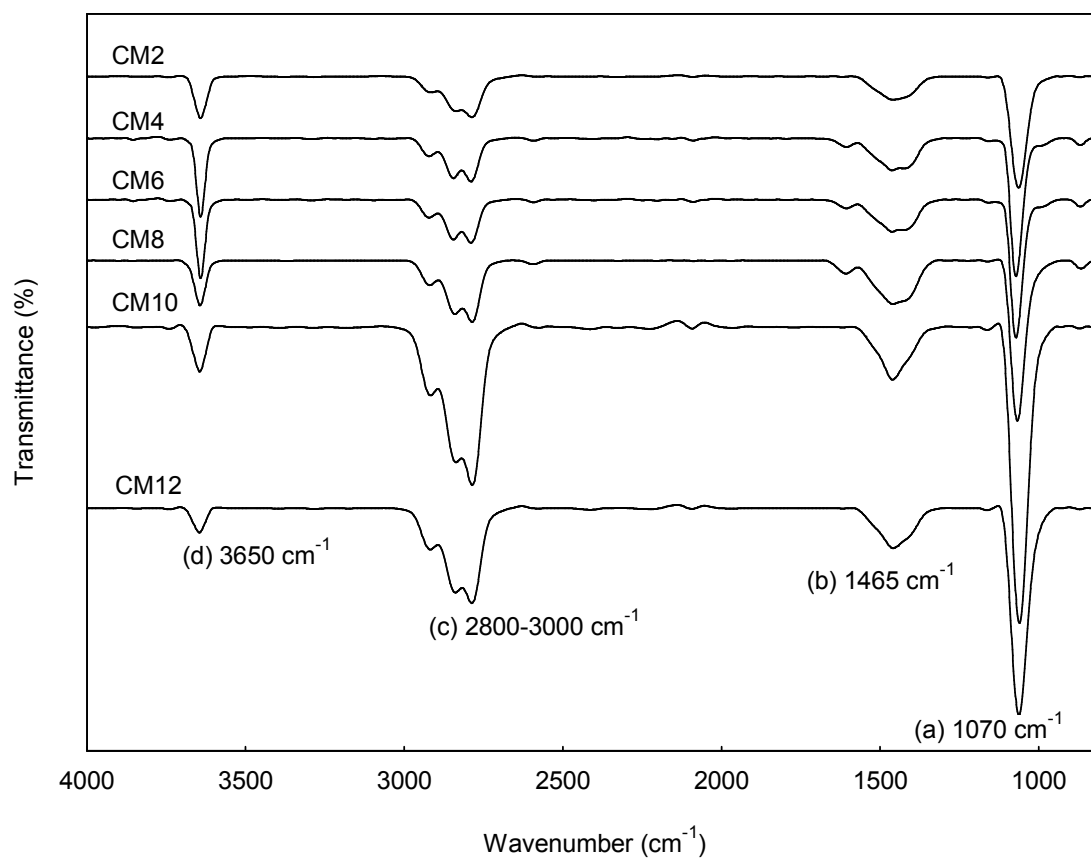
Fig. 5 FTIR spectrum of calcium methoxide catalysts.

88

89

90

g)

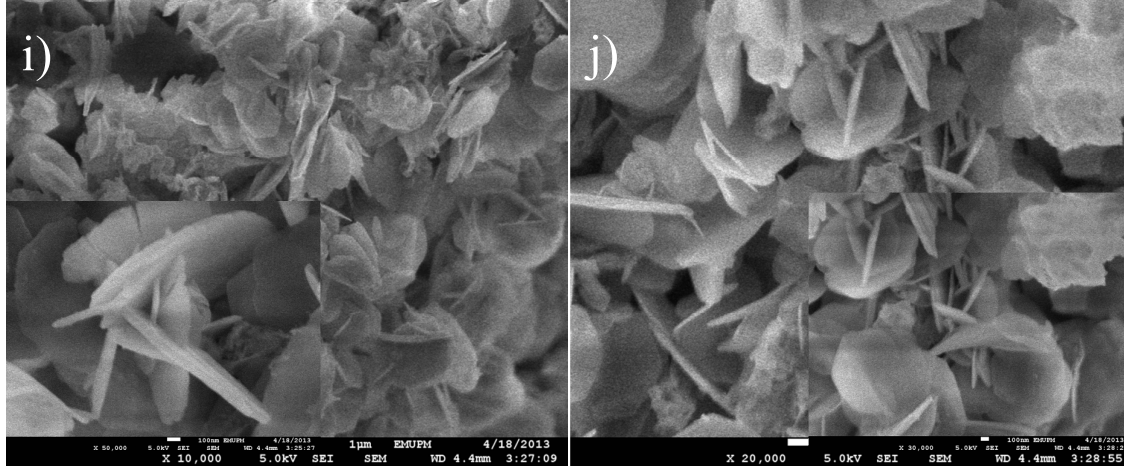*500 nm*

h)

500 nm

91

i)

1000 nm

j)

500 nm

92

k)

500 nm

l)

500 nm

93
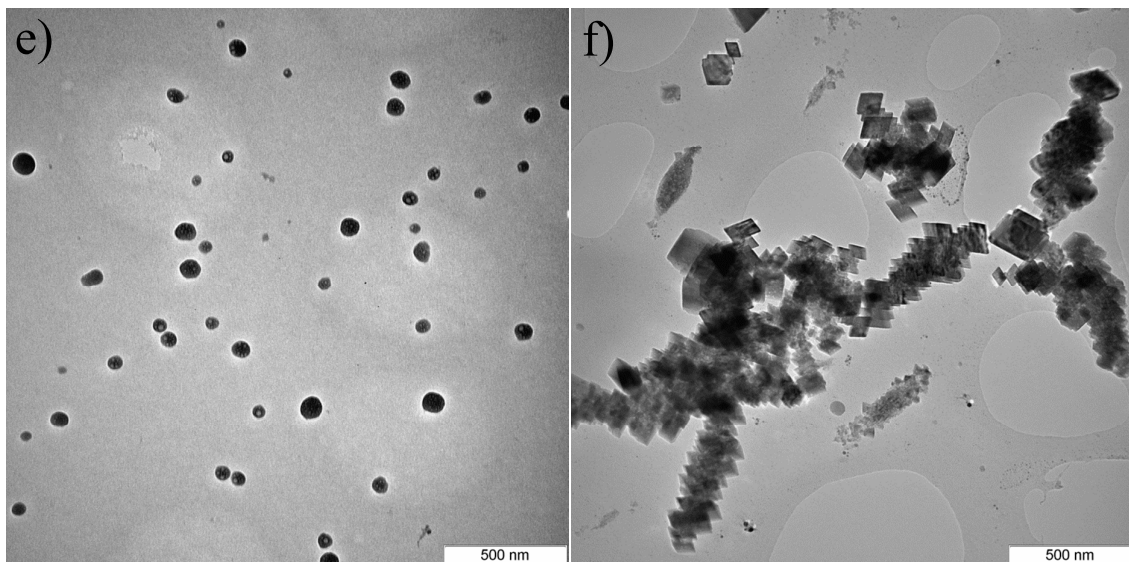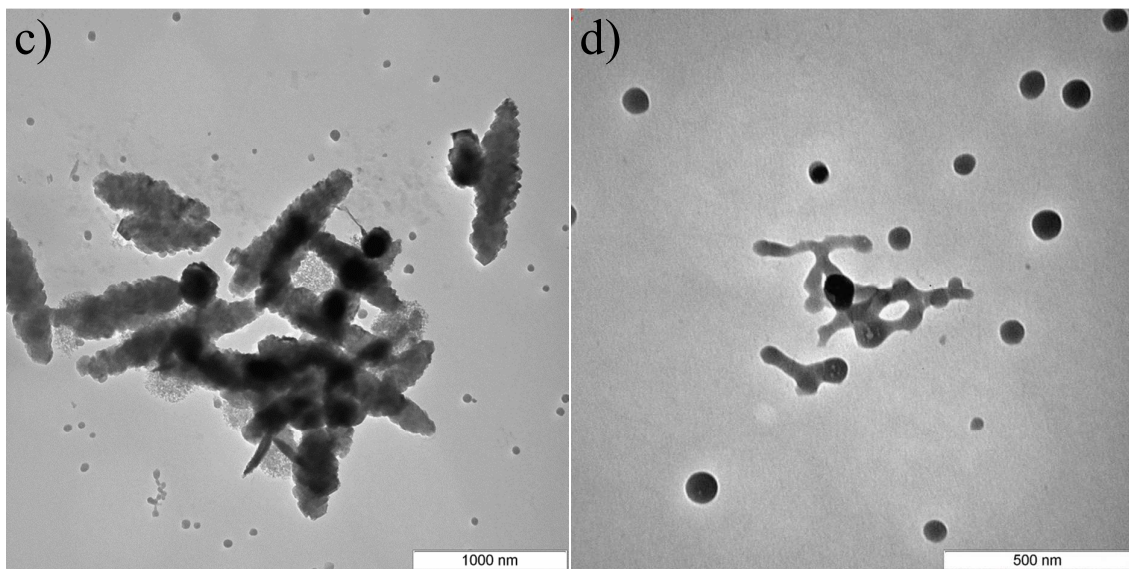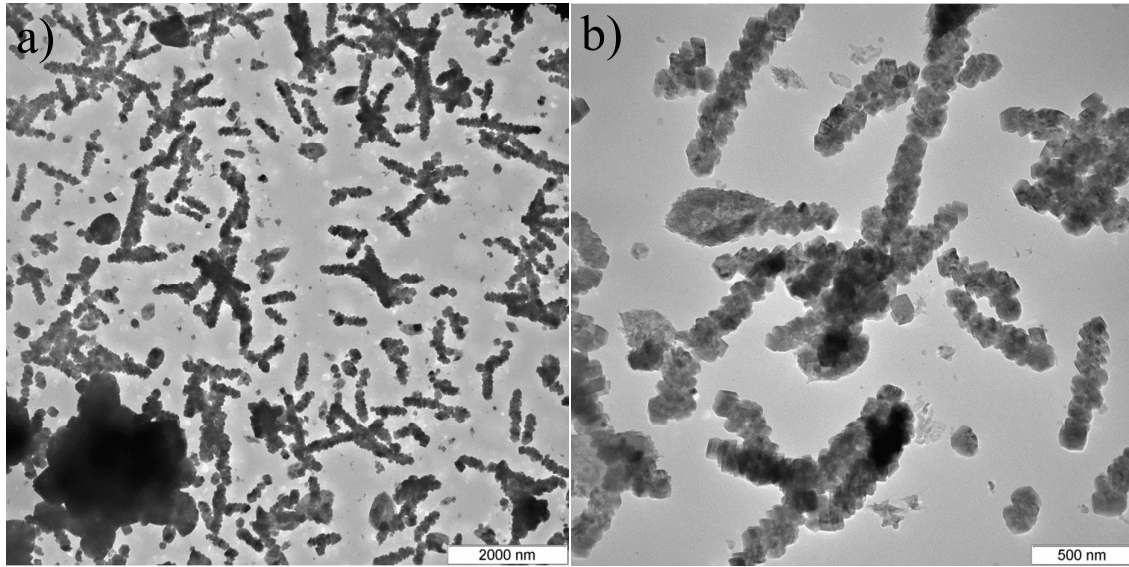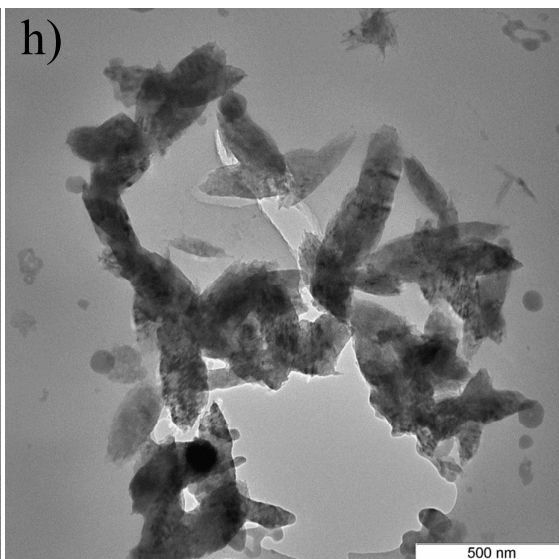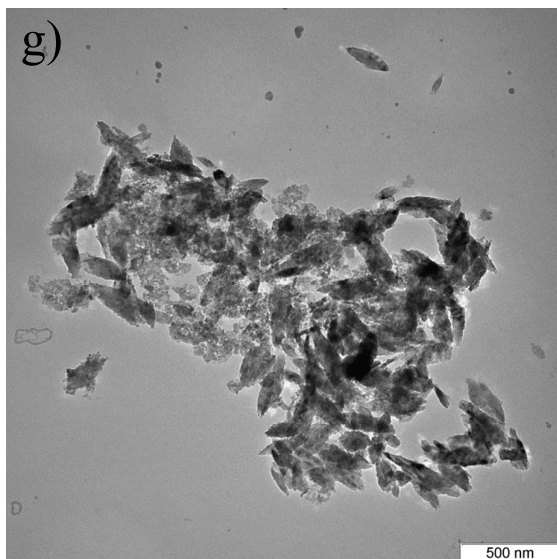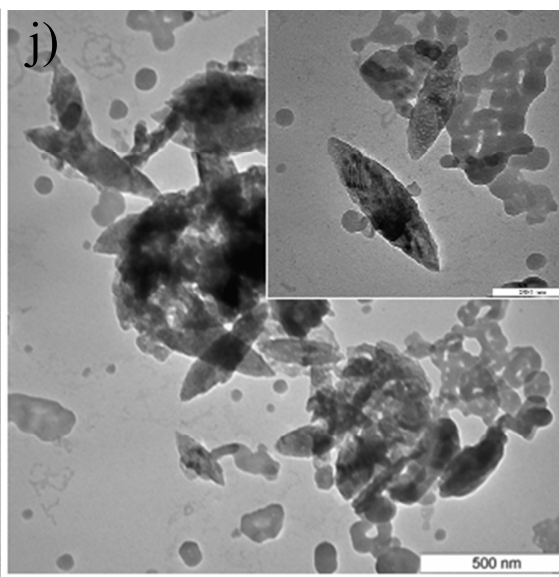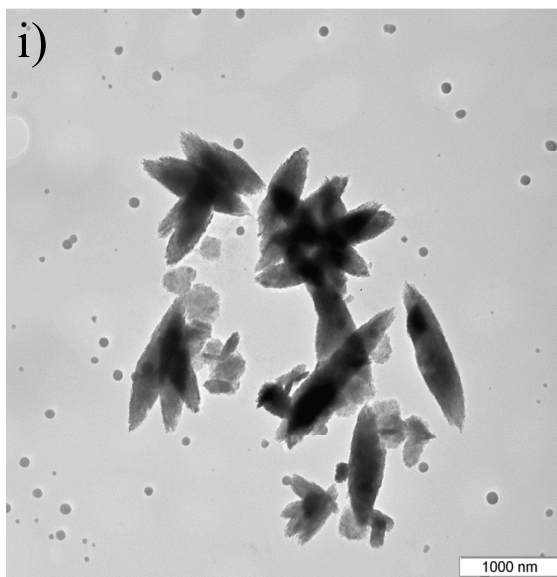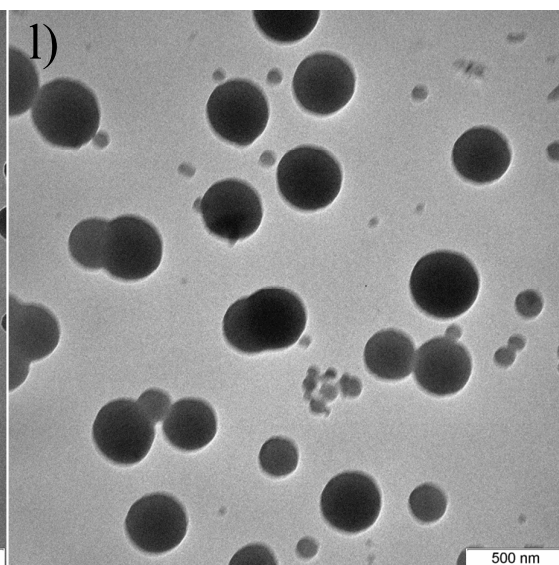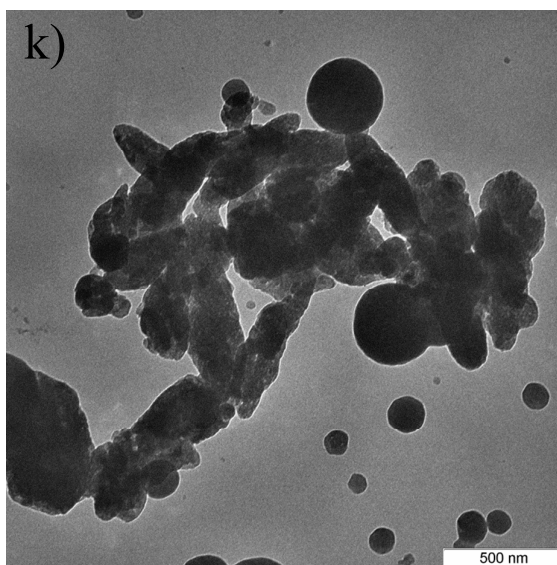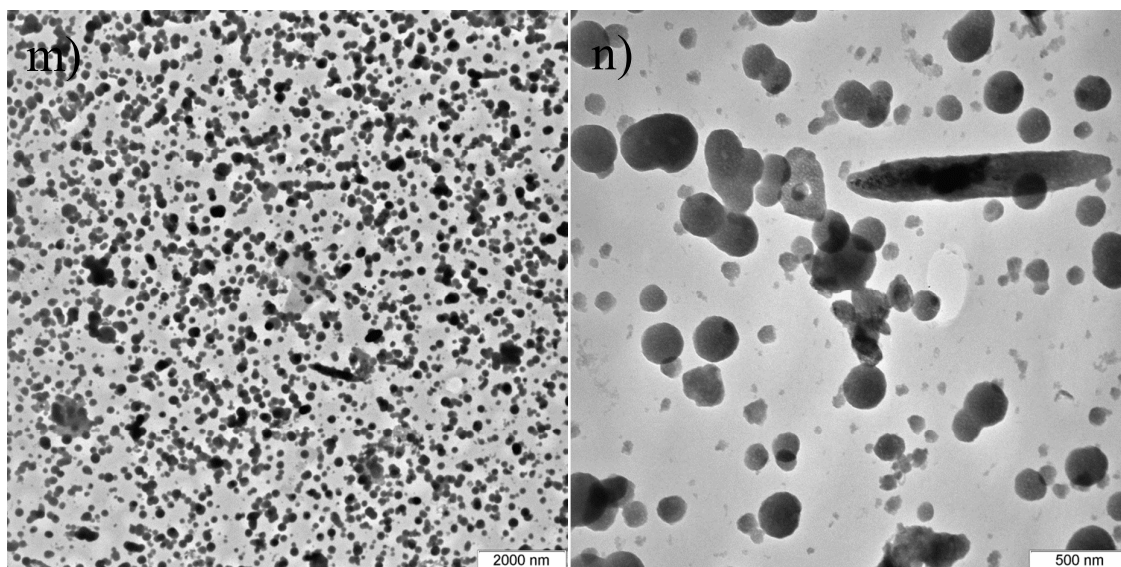
Fig. 6 TEM micrographs of calcium oxide and calcium methoxide catalysts: (a) & (b) CaO; (c) & (d) CM2; (e) & (f) CM4; (g) & (h) CM6; (i) & (j) CM8; (k) & (l) CM10 and (m) & (n) CM12.
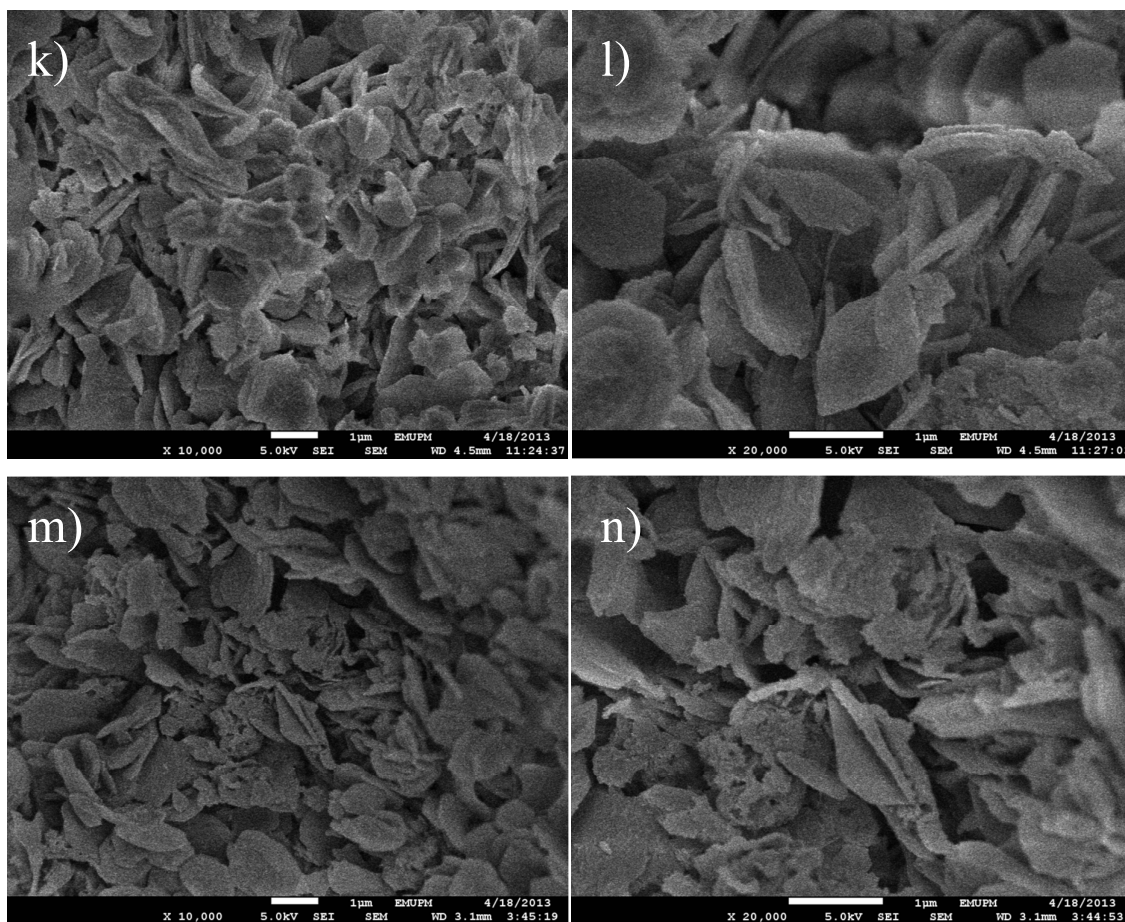
117

118

119

120

121

122
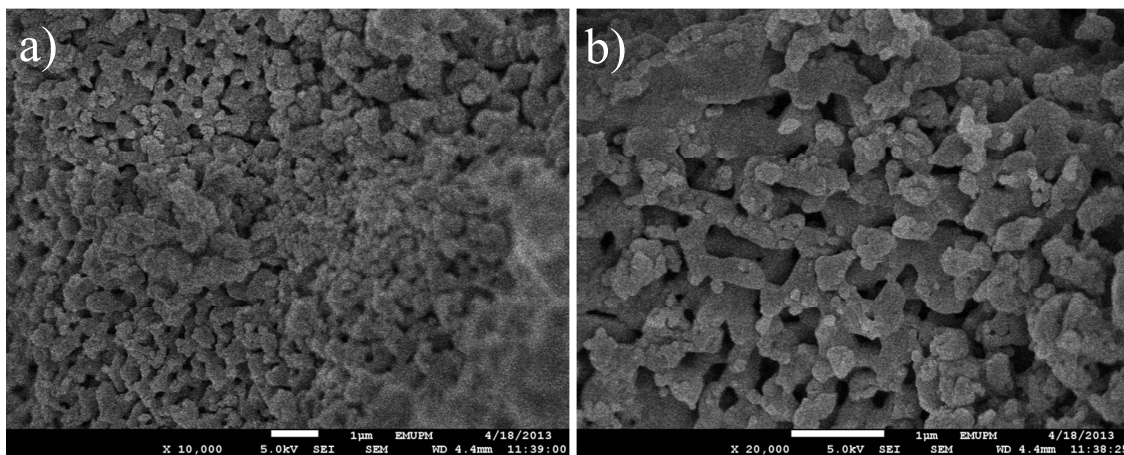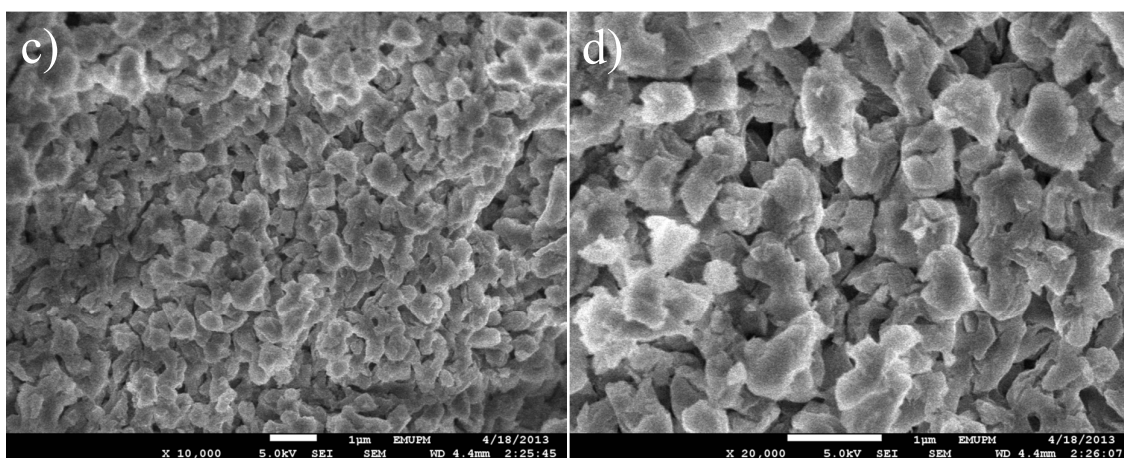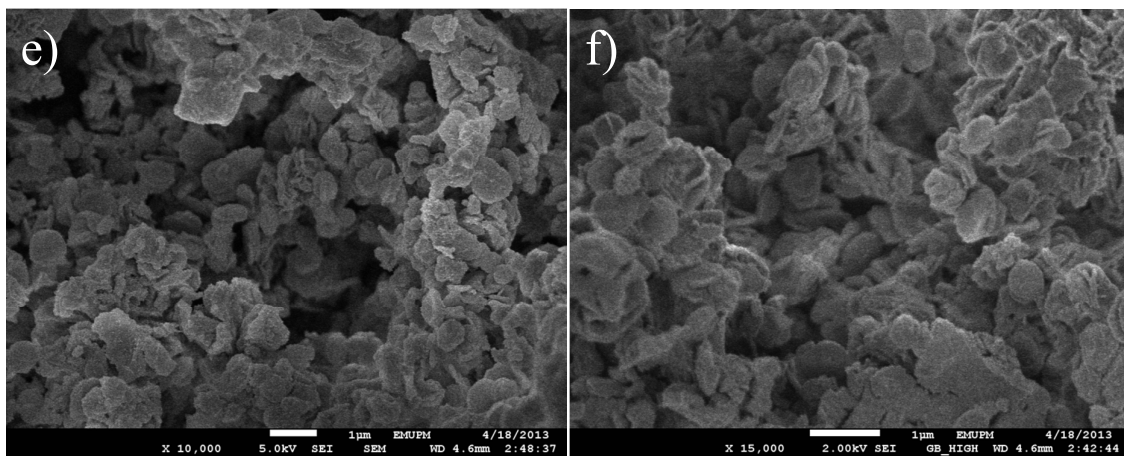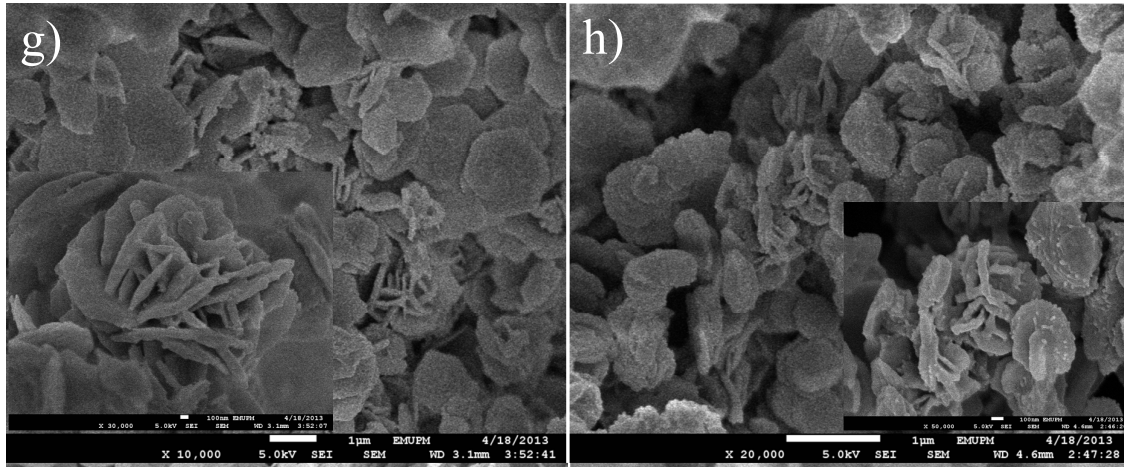
Fig. 7 SEM micrographs of calcium oxide and calcium methoxide catalysts: (a) & (b) CaO; (c) & (d) CM2; (e) & (f) CM4; (g) & (h) CM6, insert of (g) & (h) are close-up view focused on one bunch of plate-like structure particles; (i) & (j) CM8, insert of (i) is enlarge image focused on a cluster of tiny plate and insert of (j) is a magnified FESEM image on a few cluster plates; (k) & (l) CM10 and (M) & (N) CM12.

140

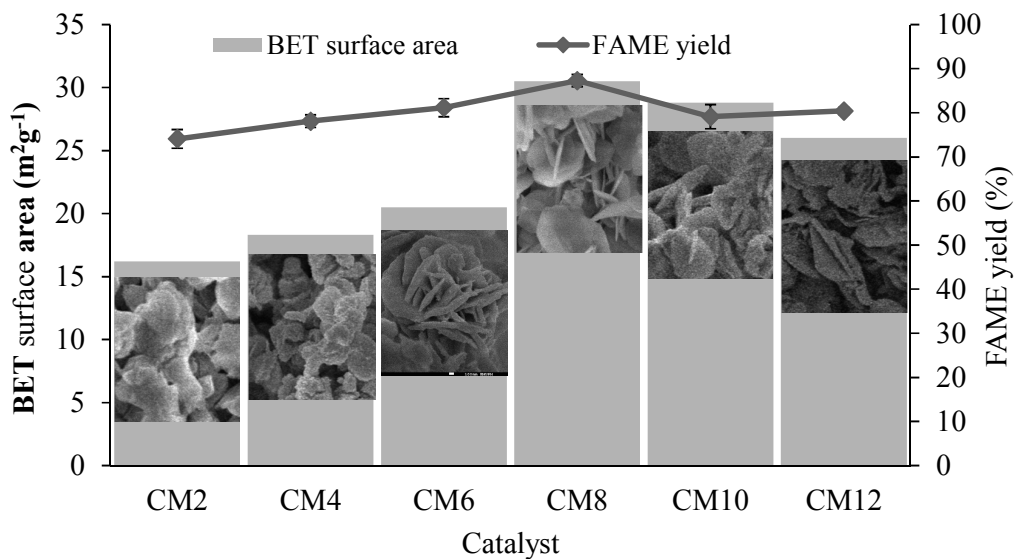141   Fig. 8 Correlation between biodiesel yield with surface area of CM2, CM4, CM6, CM8,

142   CM10 and CM12 catalysts. Reaction condition: Oil = 10 g, catalyst dosage = 2 %,

143   n(methanol):n(oil) = 12:1, reaction time = 1.5 h, reaction temperature = 65 °C.

144

145

146

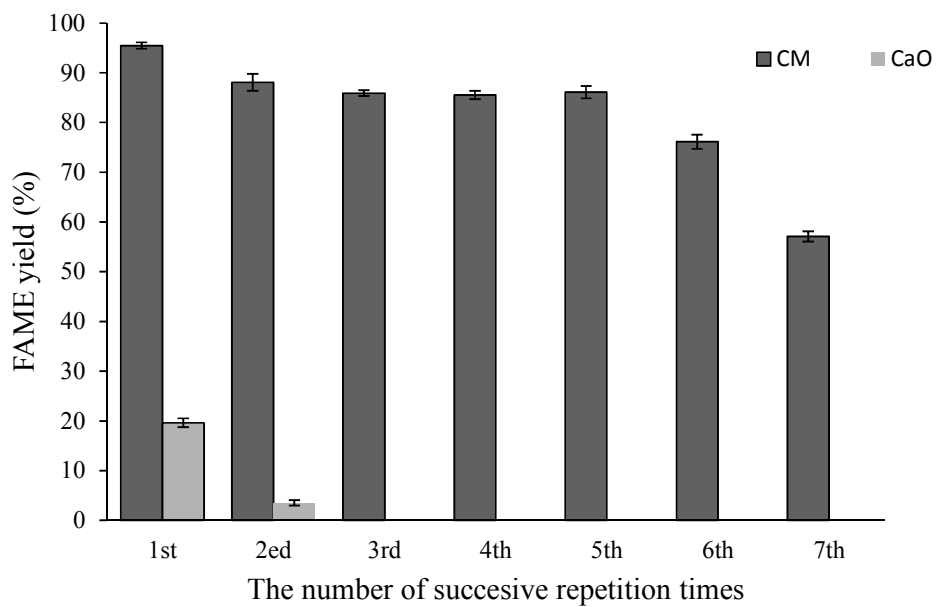147

148

149

150

151

152

153

154

155

156

157

158

159

160

161

162

163   Fig. 9 Recyclability study of CM8 and CaO catalysts. Reaction condition: Oil = 10 g, catalyst

164   dosage = 2 %, n(methanol):n(oil) = 15:1, reaction time = 1.5 h, reaction temperature = 65 °C.

165

166